

An Optimal Decoding Strategy for Physical-layer Network Coding over Multipath Fading Channel

Minglong Zhang, Lu Lu, *Member, IEEE*,
and Soung Chang Liew, *Fellow, IEEE*

Abstract

We present an optimal decoder for physical-layer network coding (PNC) in a multipath fading channel. Previous studies on PNC have largely focused on the single path case. For PNC, multipath not only introduces inter-symbol interference (ISI), but also cross-symbol interference (Cross-SI) between signals simultaneously transmitted by multiple users. In this paper, we assume the transmitters do not have channel state information (CSI). The relay in the PNC system, however, has CSI. The relay makes use of a belief propagation (BP) algorithm to decode the multipath-distorted signals received from multiple users into a network-coded packet. We refer to our multipath decoding algorithm as MP-PNC. Our simulation results show that, benchmarked against synchronous PNC over a one-path channel, the bit error rate (BER) performance penalty of MP-PNC under a two-tap ITU channel model can be kept within 0.5 dB. Moreover, it outperforms a MUD-XOR algorithm by 3dB – MUD-XOR decodes the individual information from both users explicitly before performing the XOR network-coding mapping. Although the framework of fading-channel PNC presented in this paper is demonstrated based on two-path and three-path channel models, our algorithm can be easily extended to cases with more than three paths.

Index Terms

physical-layer network coding, multipath fading, symbol misalignment, belief propagation, asynchrony

M. Zhang and L. Lu are with the Institute of Network Coding, The Chinese University of Hong Kong. S. C. Liew is with the Department of Information Engineering, The Chinese University of Hong Kong, Hong Kong. e-mails: {mlzhang, lulu, soung}@ie.cuhk.edu.hk

Corresponding to: lulu@ie.cuhk.edu.hk

I. INTRODUCTION

We investigate a two-way relay multipath channel where two end nodes A and B exchange information via a relay node R , as shown in Fig. 1. We assume half-duplex operation and no direct channel between A and B . A question is what is the minimum number of timeslots needed for the exchange of two packets between A and B via R ? Physical-layer network coding (PNC) [1] requires only two time slots: one for simultaneous uplink transmissions of A and B to R , and one for broadcast downlink transmission of R to A and B . The key lies in the uplink phase, in which the relay detects the XOR of the symbols transmitted by A and B rather than their individual symbols.

Previous studies of PNC mostly assume the single-path fading channel. This paper considers the more general multipath fading channel. With multipath, the superposition of duplicate packets arriving at the relay node results in inter-symbol interference (ISI).

Furthermore, in *asynchronous* PNC [2] [3], symbols of the A and B may arrive at the relay with symbol misalignment and carrier phase offset (for both the single-path and multipath scenarios). These asynchronies between A and B , if not properly dealt with, will lead to significant performance penalties [4]. Although [2] and [3] provided methods to reduce these performance penalties, only the single path scenario was considered. With multipath, the asynchrony problem is compounded: there are multiple symbol misalignments and carrier phase offsets between the symbols of the two transmitters. In particular, in addition to intra-user ISI, there is also Cross-SI between the two users. This paper establishes an optimal decoding framework for dealing with the ISI and Cross-SI.

Related Work

Multipath and asynchrony are both pervasive in real systems. Lu and Liew [2], [3] proposed an optimal decoding algorithm that jointly solves the phase and symbol asynchrony problem in PNC in the AWGN channel. However, the multipath scenario was not treated.

Paper [5] developed a decoding strategy for PNC over frequency selective channels in the time domain, but the work assumes the delays of the paths from node A to relay R are pairwise equal to the delays of the paths from node B to relay R (i.e., for each path for the former there is a corresponding path for the latter with the same delay, and vice versa). This assumption of pairwise-equal path delays is not realistic in real physical situations. We note in particular that in the multipath scenario, it is not possible to control the transmission times of the two end nodes to ensure that the signals on each and every paths are aligned. Thus,

for time-domain solutions, multipath PNC will necessarily be asynchronous PNC by nature.

Ref. [6] provided a frequency-domain OFDM solution for multipath PNC. Because the relative delay between the two collided packets (including the replicas due to multipath fading) is smaller than the cyclic prefix length, the channel is transformed to a flat fading model within each and every of the subcarrier. This effectively turns the time-domain asynchronous channel into multiple frequency-domain synchronous channels [7]. Although frequency-domain PNC can solve the symbol asynchrony problem, its performance is sensitive to the carrier frequency offset (CFO) between the two end nodes [8].

Contributions

To the best of our knowledge, no prior studies have considered the time-domain asynchronous PNC over multipath fading channels. This paper is the first to treat all the signals from multiple paths as useful information to be exploited in PNC decoding. In particular, we derive a maximum-likelihood (ML) optimal decoding algorithm based on the belief propagation (BP) algorithm that can make best use of the signals arriving from the respective multiple paths of the two users to decode for a network-coded packet. Extensive simulations indicate that the BER performance penalty can be kept within 0.5 dB compared with that of synchronous PNC in an AWGN channel. Moreover, for different phase offsets, we can adopt different mapping rules to ensure the best performance of the system.

The remainder of this paper is organized as follows: Section II describes the system model. Section III presents the proposed optimal multipath PNC decoding algorithm. Numerical results are given in Section IV. Section V concludes this paper.

II. SYSTEM MODEL

We study a two-way relay multipath channel network, as shown in Fig. 1. Two end nodes A and B exchange information via a relay R in the middle. We assume all nodes are half-duplex and there is no direct link between two end nodes. We adopt a two-phase transmission scheme. In this scheme, nodes A and B transmit packets to relay R simultaneously in the first phase; R then constructs a new network-coded packet based on the collided signals and broadcasts it to both A and B in the second phase. After receiving the downlink packet, A (B) can decode B 's packet (A 's packet) by subtracting its own packet (i.e., using XOR operation [1]).

For convenience, we express time in units of symbol durations. That is, the duration of one symbol is 1 here. Each symbol is carried on a rectangular pulse $g(t) = \text{rect}(t) =$

$$u(t+1) - u(t).$$

The number of paths from A to R is p , and the number of paths from B to R is s . Each path attenuates, delays, and introduces a phase shift to the original transmitted signals. Let $c_i^A(t) = \eta_i e^{j\varphi_i} \delta(t)$ be the channel impulse response of path i of node A , and $c_j^B(t) = \mu_j e^{j\theta_j} \delta(t)$ be the channel impulse response of path j of node B ¹, where $\eta_i(\mu_j)$ and $\varphi_i(\theta_j)$ are attenuation factors and phase shifts of path $i(j)$, for node $A(B)$, respectively. Then, the overall impulse response of path i of node A , taking into consideration the pulse shape $g(t)$, is $h_i^A(t) = \int_{-\infty}^{+\infty} g(\tau) c_i^A(t - \tau) d\tau$; similarly, the overall impulse response of path j of node B is $h_j^B(t) = \int_{-\infty}^{+\infty} g(\tau) c_j^B(t - \tau) d\tau$. In other words, $h_i^A(t)$ and $h_j^B(t)$ are the effective pulse shapes.

Let τ_i be the delay of path i of node A , and $l_j + \Delta$ ($0 < \Delta < 1$) be the delay of path j of node B . Without loss of generality, we assume $\tau_0 < \tau_1 < \dots < \tau_{p-1}$ and $l_0 < l_1 < \dots < l_{s-1}$, and we further set $\tau_0 = 0$ and $l_0 = 0$ so that Δ is the relative delay by which the first path of node A is ahead of the first path of node B . Then, the overall received complex baseband signal at the relay can be expressed as

$$r(t) = \sum_{n=1}^N \left\{ \sum_{i=0}^{p-1} x_A[n] h_i^A(t - (n + \tau_i)) + \sum_{j=0}^{s-1} x_B[n] h_j^B(t - (n + l_j + \Delta)) \right\} + w(t), \quad (1)$$

where $x_A[n]$ and $x_B[n]$ are the symbols of nodes A and B , respectively, and $w(t)$ is the additive white Gaussian noise with double-sided power spectrum density $N_0/2$.

We further assume that $0 < \tau_i \leq 1$ and $0 < l_j \leq 1 - \Delta$ for all $i, j > 0$. That is, the delay spread of all paths (from A as well as B) is within one symbol duration. This assumption of the delay spread is in accordance with some actual environments as specified in the guidelines in ITU-R Recommendation M.1225 [9]. For example, in a three-tap channel model of the indoor office, the delay for each tap is less than 100ns. It means this assumption is suitable for a system in which the transmission rate is no more than 10Mbaud per second.

For simplicity, we first consider the case where there are only two paths between each end node and the relay. We will show later that our method is extendable to cases with three or more paths. Then (1) can be simplified to

$$r(t) = \sum_{n=1}^N \left\{ \sum_{i=0}^1 x_A[n] h_i^A(t - (n + \tau_i)) + \sum_{j=0}^1 x_B[n] h_j^B(t - (n + l_j + \Delta)) \right\} + w(t). \quad (2)$$

¹Note that here $c_i^A(t)$ and $c_j^B(t)$ have not included the path delays yet. We only model how the pulse shape $g(t)$ is changed by the channel here. Path delays will be taken into consideration in eqn. (1).

A crucial question is how relay R can generate a network-coded packet from the noisy overlapped signal $r(t)$. This paper proposes a two-step decoding algorithm: 1) first oversamples $r(t)$; and 2) use these discrete samples to build a Tanner Graph to compute the maximum *a posteriori* probability (MAP) for the network-coded packet.

For 1), we consider two oversampling methods described in the following paragraphs:

Method I: double sampling

Method I passes the overlapped signals $r(t)$ through two parallel matched filters and then samples their outputs at time instants $(n - 1 + \Delta)$ and n , $n = 1, 2, \dots, N$, respectively. We get the following discrete-time samples:

$$\begin{aligned} r[2n - 1] &= \frac{1}{\Delta} \int_{(n-1)}^{(n-1)+\Delta} r(t) h_A^*(t) dt = x_A[n] \rho_{aa}^0 + x_A[n - 1] \rho_{aa}^1 + x_B[n - 1] \rho_{ab} + w[2n - 1]; \\ r[2n] &= \frac{1}{1 - \Delta} \int_{(n-1)+\Delta}^n r(t) h_B^*(t) dt = x_B[n] \rho_{bb}^0 + x_B[n - 1] \rho_{bb}^1 + x_A[n] \rho_{ba} + w[2n], \end{aligned} \quad (3)$$

where $h_A^*(t) = (h_0^A(t) + h_1^A(t - \tau_1))^*$, $h_B^*(t) = (h_0^B(t - \Delta) + h_1^B(t - \Delta - l_1))^*$ and $\rho_{aa}^i, \rho_{bb}^i, \rho_{ab}$ and ρ_{ba} ($i = 0, 1$) are integration coefficients of the corresponding matched filters. Their definitions are

$$\begin{aligned} \rho_{aa}^0 &= \frac{1}{\Delta} \int_{(n-1)}^{(n-1)+\Delta} h_A(t - n) h_A^*(t - n) dt; \\ \rho_{aa}^1 &= \frac{1}{\Delta} \int_{(n-1)}^{(n-1)+\tau_1} h_1^A(t - (n - 1 + \tau_1)) h_A^*(t - n) dt; \\ \rho_{ab} &= \frac{1}{\Delta} \int_{(n-1)}^{(n-1)+\Delta} [h_{l_0}^B(t - (n - 1) - \Delta) + h_{l_1}^B(t - (n - 1) - \Delta - l_1)] h_A^*(t - n) dt; \\ \rho_{bb}^0 &= \frac{1}{1 - \Delta} \int_{(n-1)+\Delta}^n h_B(t - n) h_B^*(t - n) dt; \\ \rho_{bb}^1 &= \frac{1}{1 - \Delta} \int_{(n-1)+\Delta}^{(n-1)+\Delta+l_1} (h_{l_1}^B(t - (n - 1) - l_1 - \Delta)) h_B^*(t - n) dt; \\ \rho_{ba} &= \frac{1}{1 - \Delta} \int_{(n-1)+\Delta}^n [h_0^A(t - n) + h_1^A(t - n - \tau_1)] h_B^*(t - n) dt. \end{aligned} \quad (4)$$

These coefficients are all independent of n , since we assume the channel gain is constant during the transmission of one frame. $w[2n - 1]$ and $w[2n]$ are zero-mean complex Gaussian noise with variance $\alpha_1 N_0 / (2\Delta^2)$ and $\alpha_2 N_0 / 2(1 - \Delta)^2$, respectively, for both the real and imaginary components. Here α_1 and α_2 are constants given by

$$\alpha_1 = \int_{n-1}^{(n-1)+\Delta} |h_A(t)|^2 dt; \quad \alpha_2 = \int_{(n-1)+\Delta}^n |h_B(t)|^2 dt. \quad (5)$$

Method II: quadruple sampling

Method II quadruples the samples. Since there is more than one path between each end node and the relay, and each path has a different channel response, we initiate a new matched filter for each path. Therefore, we adopt a fourfold sampling method at the relay. The received signal $r(t)$ serves as the input to the four different matched filters. The outputs are sampled at time instants $(n-1+\tau_1)$, $(n-1+\Delta)$, $(n-1+\Delta+l_1)$ and n ($n = 1, 2, \dots, N$), accordingly. The samples are as follows:

$$\begin{aligned} r[4n-3] &= \frac{1}{\tau_1} \int_{(n-1)}^{(n-1)+\tau_1} r(t) h_0^A(t-n) dt = x_A[n] \mu_{aa}^0 + x_A[n-1] \mu_{aa}^1 + x_B[n-1] (\mu_{ab}^0 + \mu_{ab}^1) + w[4n-3]; \\ r[4n-2] &= \frac{1}{\Delta - \tau_1} \int_{(n-1)+\tau_1}^{(n-1)+\Delta} r(t) h_1^A(t-(n+\tau_1)) dt = x_A[n] (\lambda_{aa}^0 + \lambda_{aa}^1) + x_B[n-1] (\lambda_{ab}^0 + \lambda_{ab}^1) + w[4n-2]; \\ r[4n-1] &= \frac{1}{l_1} \int_{(n-1)+\Delta}^{(n-1)+\Delta+l_1} r(t) h_0^B(t-(n+\Delta)) dt = x_A[n] (\mu_{ba}^0 + \mu_{ba}^1) + x_B[n] \mu_{bb}^0 + x_B[n-1] \mu_{bb}^1 + w[4n-1]; \\ r[4n] &= \frac{1}{1 - \Delta - l_1} \int_{(n-1)+\Delta+l_1}^n r(t) h_1^B(t-(n+l_1+\Delta)) dt = x_A[n] (\lambda_{ba}^0 + \lambda_{ba}^1) + x_B[n] (\lambda_{bb}^0 + \lambda_{bb}^1) + w[4n], \quad (6) \end{aligned}$$

where $\mu_{aa}^i, \mu_{ab}^i, \mu_{ba}^i, \mu_{bb}^i, \lambda_{aa}^i, \lambda_{ab}^i, \lambda_{ba}^i$ and λ_{bb}^i ($i = 0, 1$) are integration coefficients from the matched filters. They have similar definitions as in (4). Analogously, $w[4n-3]$, $w[4n-2]$, $w[4n-1]$ and $w[4n]$ are zero-mean complex Gaussian noise with variance $\beta_1 N_0 / 2\tau_1^2$, $\beta_2 N_0 / 2(\Delta - \tau_1)^2$, $\beta_3 N_0 / 2l_1^2$ and $\beta_4 N_0 / 2(1 - \Delta - l_1)^2$, respectively, for both the real and imaginary components. $\beta_1, \beta_2, \beta_3$ and β_4 are constants and can be computed like equation (5).

III. JOINT DECODING SCHEME AT THE RELAY

This section presents our decoding scheme based on the BP algorithm for PNC under multipath conditions. We refer to our algorithm as MP-PNC. We assume that the relay node, by means of preambles, can perfectly estimate the channel state information (CSI), including channel impulse responses $h_i^A(t)$ and $h_j^B(t)$, symbol timing offset Δ , and propagation delays τ_i and l_j in (2). We compute the coefficients ρ, λ and μ in (3) and (6). Note that the phase differences between different users and different multipath channel taps are embedded in ρ, λ and μ already. In order to decode the joint symbol $(x_A[n], x_B[n])$, $n = 1, 2, \dots, N$, from (3) or (6), we need to look at $\Pr(x_A[n], x_B[n] | r_1, r_2, \dots, r_{2N})$ or $\Pr(x_A[n], x_B[n] | r_1, r_2, \dots, r_{4N})$, respectively. To simplify notation, let $x_A^n x_B^n$ and r_i denote $(x_A[n], x_B[n])$ and $r[i]$, respectively; and let r denote r_1, r_2, \dots, r_{2N} in (3) or r_1, r_2, \dots, r_{4N} in (6). We use a BP decoding algorithm to find the exact *a posteriori* probability $\Pr(x_A^n x_B^n | r)$. From this decoded probability, we can compute the maximum *a posteriori* probability (MAP) XOR value for the downlink packet

as follows:

$$x_R[n] = \arg \max_x \Pr(x_A[n] \oplus x_B[n] = x|r) = \arg \max_x \sum_{x_A^n x_B^n : x_A[n] \oplus x_B[n] = x} \Pr(x_A^n x_B^n | r). \quad (7)$$

The proposed MP-PNC decoding scheme is a maximum likelihood (ML) decoder, and hence optimal in terms of BER.

A. Tanner graph construction

Based on the relationships among the received samples in (3) and (6), we construct a Tanner graph as shown in Fig. 2(a) and Fig. 2(b), respectively. In Fig. 2(a), X_1, X_2, \dots , and X_{2N} denote the $2N$ variable nodes, and each X_i is associated with a cluster of adjacent symbols from nodes A and B whose information is contained in sample r_i . Thus, X_i is connected to the evidence node associated with sample r_i . Compatibility (or factor) nodes ψ represent the connectivity among different variable nodes. Similar notations are adopted by Fig. 2(b) for the quadruple sampling case.

The Tanner graph in Fig. 2 is a Markov process: e.g., $\Pr(X_i | X_{i-1} X_{i-2}) = \Pr(X_i | X_{i-1})$. That is, given X_{i-1} , X_i is independent of X_{i-2} .

For message passing from left to right, the definition of the compatibility function between variable node X_{i-1} and X_i in Fig. 2 is

$$\psi(X_{i-1}, X_i) \propto \Pr(X_{i-1} | X_i). \quad (8)$$

Our final goal is to decode the probability $\Pr(x_A^n x_B^n | r)$, from which we can obtain the ML network-coded symbol $x_R[n] = x_A[n] \oplus x_B[n]$. We first calculate $P_{2n-1}(x_A^n x_A^{n-1} x_B^{n-1} | r[2n-1])$ and $P_{2n}(x_A^n x_B^n x_B^{n-1} | r[2n])$ from (3). Similarly, we compute the probability $P_{4n-3}(x_A^n x_A^{n-1} x_B^{n-1} | r[4n-3])$, $P_{4n-2}(x_A^n x_B^{n-1} | r[4n-2])$, $P_{4n-1}(x_A^n x_B^n x_B^{n-1} | r[4n-1])$, and $P_{4n}(x_A^n x_B^n | r[4n])$ from (6).

Denote the symbol set for QPSK modulation by $\chi = \{1 + j, -1 + j, -1 - j, 1 - j\}$. Let a, b and $c \in \chi$, the probabilities for the evidence node $2n-1$ and $2n$ in Fig. 2(a) are calculated as follows:

$$\begin{aligned} p_{2n-1}^{a,b,c} &= P\left(x_A[n] = \frac{a}{\sqrt{2}}, x_B[n-1] = \frac{b}{\sqrt{2}}, x_A[n-1] = \frac{c}{\sqrt{2}} | r[2n-1]\right) \\ &\propto \frac{1}{2\pi\alpha_1\sigma^2/\Delta^2} \cdot \exp\left\{-\frac{\left(\text{Re}(r[2n-1]) - \text{Re}(\rho_{aa}^0 \cdot a + \rho_{ab} \cdot b + \rho_{aa}^1 \cdot c) / \sqrt{2}\right)^2}{2\alpha_1\sigma^2/\Delta^2}\right\} \\ &\quad \exp\left\{-\frac{\left(\text{Im}(r[2n-1]) - \text{Im}(\rho_{aa}^0 \cdot a + \rho_{ab} \cdot b + \rho_{aa}^1 \cdot c) \sqrt{2}\right)^2}{2\alpha_1\sigma^2/\Delta^2}\right\}; \end{aligned}$$

$$\begin{aligned}
p_{2n}^{a,c,b} &= P\left(x_A[n] = \frac{a}{\sqrt{2}}, x_B[n] = \frac{c}{\sqrt{2}}, x_B[n-1] = \frac{b}{\sqrt{2}}|r[2n]\right) \\
&\propto \frac{1}{2\pi\alpha_2\sigma^2/(1-\Delta)^2} \cdot \exp\left\{-\frac{\left(\text{Re}(r[2n]) - \text{Re}(\rho_{ba} \cdot a + \rho_{bb}^0 \cdot c + \rho_{bb}^1 \cdot b) / \sqrt{2}\right)^2}{2\alpha_2\sigma^2/(1-\Delta)^2}\right\} \\
&\quad \exp\left\{-\frac{\left(\text{Im}(r[2n]) - \text{Im}(\rho_{ba} \cdot a + \rho_{bb}^0 \cdot c + \rho_{bb}^1 \cdot b) / \sqrt{2}\right)^2}{2\alpha_2\sigma^2/(1-\Delta)^2}\right\}, \tag{9}
\end{aligned}$$

where the coefficients are given in (4) and (5). $\text{Re}(\cdot)$ and $\text{Im}(\cdot)$ denote the real and imaginary parts of the signal, respectively. Similarly, for quadruple sampling in Fig. 2(b), we have

$$\begin{aligned}
p_{4n-3}^{a,b,c} &= P\left(x_A[n] = \frac{a}{\sqrt{2}}, x_B[n-1] = \frac{b}{\sqrt{2}}, x_A[n-1] = \frac{c}{\sqrt{2}}|r[4n-3]\right) \\
&\propto \frac{1}{2\pi\beta_1\sigma^2/\tau_1^2} \cdot \exp\left\{-\frac{\left(\text{Re}(r[4n-3]) - \text{Re}(\mu_{aa}^0 \cdot a + (\mu_{ab}^0 + \mu_{ab}^1) \cdot b + \mu_{aa}^1 \cdot c) / \sqrt{2}\right)^2}{2\beta_1\sigma^2/\tau_1^2}\right\} \\
&\quad \exp\left\{-\frac{\left(\text{Im}(r[4n-3]) - \text{Im}(\mu_{aa}^0 \cdot a + (\mu_{ab}^0 + \mu_{ab}^1) \cdot b + \mu_{aa}^1 \cdot c) / \sqrt{2}\right)^2}{2\beta_1\sigma^2/\tau_1^2}\right\}; \\
p_{4n-2}^{a,b} &= P\left(x_A[n] = \frac{a}{\sqrt{2}}, x_B[n-1] = \frac{b}{\sqrt{2}}|r[4n-2]\right) \\
&\propto \frac{1}{2\pi\beta_2\sigma^2/(\Delta - \tau_1)^2} \cdot \exp\left\{-\frac{\left(\text{Re}(r[4n-2]) - \text{Re}((\lambda_{aa}^0 + \lambda_{aa}^1) \cdot a + (\lambda_{ab}^0 + \lambda_{ab}^1) \cdot b) / \sqrt{2}\right)^2}{2\beta_2\sigma^2/(\Delta - \tau_1)^2}\right\} \\
&\quad \exp\left\{-\frac{\left(\text{Im}(r[4n-2]) - \text{Im}((\lambda_{aa}^0 + \lambda_{aa}^1) \cdot a + (\lambda_{ab}^0 + \lambda_{ab}^1) \cdot b) / \sqrt{2}\right)^2}{2\beta_2\sigma^2/(\Delta - \tau_1)^2}\right\}; \\
p_{4n-1}^{a,c,b} &= P\left(x_A[n] = \frac{a}{\sqrt{2}}, x_B[n] = \frac{c}{\sqrt{2}}, x_B[n-1] = \frac{b}{\sqrt{2}}|r[4n-1]\right) \\
&\propto \frac{1}{2\pi\beta_3\sigma^2/l_1^2} \cdot \exp\left\{-\frac{\left(\text{Re}(r[4n-1]) - \text{Re}((\mu_{ba}^0 + \mu_{ba}^1) \cdot a + \mu_{bb}^0 \cdot c + \mu_{bb}^1 \cdot b) / \sqrt{2}\right)^2}{2\beta_3\sigma^2/l_1^2}\right\} \\
&\quad \exp\left\{-\frac{\left(\text{Im}(r[4n-1]) - \text{Im}((\mu_{ba}^0 + \mu_{ba}^1) \cdot a + \mu_{bb}^0 \cdot c + \mu_{bb}^1 \cdot b) / \sqrt{2}\right)^2}{2\beta_3\sigma^2/l_1^2}\right\}; \\
p_{4n}^{a,c} &= P\left(x_A[n] = \frac{a}{\sqrt{2}}, x_B[n] = \frac{c}{\sqrt{2}}|r[4n]\right) \\
&\propto \frac{1}{2\pi\beta_4\sigma^2/(1-\Delta-\tau_1)^2} \cdot \exp\left\{-\frac{\left(\text{Re}(r[4n]) - \text{Re}((\lambda_{ba}^0 + \lambda_{ba}^1) \cdot a + (\lambda_{bb}^0 + \lambda_{bb}^1) \cdot c) / \sqrt{2}\right)^2}{2\beta_4\sigma^2/(1-\Delta-\tau_1)^2}\right\} \\
&\quad \exp\left\{-\frac{\left(\text{Im}(r[4n]) - \text{Im}((\lambda_{ba}^0 + \lambda_{ba}^1) \cdot a + (\lambda_{bb}^0 + \lambda_{bb}^1) \cdot c) / \sqrt{2}\right)^2}{2\beta_4\sigma^2/(1-\Delta-\tau_1)^2}\right\}. \tag{10}
\end{aligned}$$

B. Message update rules

We make use of the message from each evidence node as in (9) and (10) to derive the message update rules for the Tanner graph in Fig. 3. The Tanner graph has a tree structure, implying only one iteration is enough (one message update on each edge) for convergence of the algorithm. We update the right-bound messages from left to right, and then the left-bound messages from right to left, as illustrated in Fig. 3. In Fig. 3, for the double sampling case, Q_k and R_k denote the right-bound and left-bound messages on the edge of the k -th compatibility node, respectively. $P_k = (p_k^{1+j,1+j,1+j}, p_k^{1+j,1+j,-1+j}, \dots, p_k^{1-j,-1-j,1-j})$ is a 64×1 probability vector, where each component is the joint conditional probability $p_k^{a,b,c}$ in (9). Similarly, $Q_{k-1} = (q_{k-1}^{1+j,1+j,1+j}, q_{k-1}^{1+j,1+j,-1+j}, \dots, q_{k-1}^{1-j,-1-j,1-j})$ and $R_k = (r_k^{1+j,1+j,1+j}, r_k^{1+j,1+j,-1+j}, \dots, r_k^{1-j,-1-j,1-j})$ are also 64×1 probability vectors where $q_{k-1}^{a,b,c}$ and $r_k^{a,b,c}$ are probabilities $P(x_A[\lceil k-1/2 \rceil] = a, x_B[\lceil k-1/2 \rceil] = c, x_B[\lfloor k-1/2 \rfloor] = b | r[1], \dots, r[k-1])$ and $P(x_A[\lfloor k/2 \rfloor] = a, x_B[\lfloor k/2 \rfloor] = c, x_B[\lceil k/2 \rceil] = b | r[1], \dots, r[k])$, respectively. Note that in Fig. 3, for Q_k and R_k , we have an arrowhead \rightarrow for the right-bound messages Q_k^{\rightarrow} and R_k^{\rightarrow} and an arrowhead \leftarrow for the left-bound messages Q_k^{\leftarrow} and R_k^{\leftarrow} . The right-bound and left-bound messages are distinct and not the same.

According to the principle of the BP algorithm (also known as the sum-product algorithm), the output of a node should be consistent with all its inputs when summing over products of all possible input combinations [10]. For our Tanner graph, the details as follows:

1) Update of right-bound messages

With reference to Fig. 3(a), suppose that we want to update Q_k^{\rightarrow} from P_K and Q_{k-1}^{\rightarrow} . Based on the sum-product principle, for each element $r_k^{a,b,c}$ in Q_k^{\rightarrow} , we compute

$$r_k^{a,b,c} = p_k^{a,b,c} \cdot q_{k-1}^{a,b,c}. \quad (11)$$

from $p_k^{a,b,c}$ and $q_{k-1}^{a,b,c}$ in P_k and Q_{k-1}^{\rightarrow} , respectively. For the input message going into the leftmost compatibility node, (11) should be $r_k^{a,b,c} = p_k^{a,b,c}$.

To update the message Q_k^{\rightarrow} from R_k^{\rightarrow} , note that Q_k^{\rightarrow} is from compatibility node ψ_k and R_k^{\rightarrow} is from variable node X_k . Suppose that for X_k and X_{k+1} , the common symbols overlapped in the two adjacent samples are a and c . Then we have

$$q_k^{a,1+j,c} = q_k^{a,-1+j,c} = q_k^{a,-1-j,c} = q_k^{a,1-j,c} = \sum_b r_k^{a,b,c}. \quad (12)$$

Similarly, if the common symbols are b and c , (or a and b), the update equation are

$$q_k^{1+j,b,c} = q_k^{-1+j,b,c} = q_k^{-1-j,b,c} = q_k^{1-j,b,c} = \sum_a r_k^{a,b,c}; \quad (13)$$

or

$$q_k^{a,b,1+j} = q_k^{a,b,-1+j} = q_k^{a,b,-1-j} = q_k^{a,b,1-j} = \sum_c r_k^{a,b,c}. \quad (14)$$

By applying the update rules described in (11)-(14), we can update the next message R_{k+1}^{\rightarrow} and Q_{k+1}^{\rightarrow} , and so on and so forth until we reach the right-most node.

2) Update of left-bound messages

With reference to Fig. 3(b), we use a similar method as in 1) to update the left-bounded messages. Moreover, for the quadruple sampling case, the message passing procedure is analogous to the double sampling case discussed.

C. Decision Making

After the message passing process, for the double sampling case, at each even evidence node we have

$$p(x_A[n] = a, x_B[n] = b, x_B[n-1] = c | r) = \mu(X_{2n}) = p_{2n}^{a,b,c} \cdot q_{2n-1}^{a,b,c} \cdot r_{2n}^{a,b,c}. \quad (15)$$

For the last node, (15) is modified by omitting $r_{2N}^{a,b,c}$. By marginalizing the variable $x_B[n-1]$, we compute the ML network-coded symbol:

$$x_R[n] = x_A[n] \oplus x_B[n] = \arg \max_{x \in \chi} \left(\sum_{x=x_A[n] \oplus x_B[n]} \sum_{x_B[n-1]} \mu(X_{2n}) \right). \quad (16)$$

For the quadruple sampling case, the decision making equation is analogous:

$$x_R[n] = x_A[n] \oplus x_B[n] = \arg \max_x \left(\sum_{x=x_A[n] \oplus x_B[n]} \mu(X_{4n}) \right). \quad (17)$$

where $\mu(X_{4n}) = p_{4n}^{a,b} \cdot q_{4n-2}^{a,b} \cdot r_{4n-1}^{a,b}$. Note that for every fourth variable node in Fig. 2(b), there only have two variables $x_A[n]$ and $x_B[n]$. Therefore, it no needs to do marginalization like (16).

D. Extension to Multipath Channel with more than Two Paths

The decoding algorithm presented in the above subsections is not only suitable for the two-tap channel model, but can also be easily extended to the multiple-tap (i.e., more than two paths) channel model. Specifically, if the number of paths is three and the last tap arrival time is still within the first symbol duration, a Tanner graph can be derived in a similar manner. For instance, we can still adopt the double sampling method to construct a Tanner graph, and

then update the messages. Let us take QPSK modulation for an example, the combination turns out to contain four variables $(x_A[n], x_A[n-1], x_B[n], x_B[n-1])$ ($n = 1, 2, \dots, N$) at most in (9) and becomes a 256×1 probability vector. Therefore, the complexity of the update rules is no more than 256 multiplications (see (11)), and other operations are simple additions. Similarly, we can extend our method to the four or more path channel. However, the computing complexity will increase quickly. In practice, in an indoor application scenario, we typically need to consider only the first three paths because the energy for the fourth path and thereafter decays quickly (its average power is less than 1% to the overall power) [9].

IV. SIMULATION RESULTS

In this section, we present the numerical simulation results for MP-PNC. The synchronous PNC without multipath [2] and an extended MUD-XOR decoding method are used as benchmarks for evaluating the average bit error rate (BER) performance. The QPSK symbol amplitude is scaled to $\sqrt{2}$ of the BPSK symbol amplitude to equalize the per-bit energy. Moreover, for fair comparison, we equalize the per-bit SNRs in the multipath system and the AWGN single-path system.

A. Channel Model

In our simulation, we adopt the empirical multipath channel model, specified in the ITU-R recommendation M.1225 [9]. In particular, we choose two different three-tap indoor office channel models as the wireless channels between two end nodes and the relay, respectively. The channel impulse responses between node A (node B) and relay R are as follows:

$$\begin{aligned} h_A(t) &= \delta(t) + 0.7079\delta(t - 0.05) + 0.3162\delta(t - 0.11) \\ h_B(t) &= \delta(t) + 0.6808\delta(t - 0.1) + 0.4365\delta(t - 0.2), \end{aligned} \quad (18)$$

where we assume the bandwidth for each channel is 1 MHz. The amplitude of the first tap is normalized 1, and the largest delay spread (i.e., the last path) is within one symbol duration. As discussed in Section III, the powers of the signals for the fourth path and thereafter are very weak, and therefore we omit them in the simulation.

B. Extended Disjoint MUD-XOR Decoding Scheme

The MP-PNC is a joint decoding algorithm. For benchmarking MP-PNC, we consider a conventional disjoint MUD-XOR decoding scheme [11] that decodes both $x_A[n]$ and

$x_B[n](n = 1, 2, \dots, N)$ individually before carrying out the XOR operation at the relay node. The disjoint decoding algorithm in [11] was based on the AWGN channel. Here we show how to extend it to a multipath system. We can treat the received samples in (3) as the outputs of a virtual convolutional encoder as shown in Fig. 4. The input stream of symbols to the encoder is $v[1]v[2]v[3]v[4]\dots = x_A[1]x_B[1]x_A[2]x_B[2]x_A[3]\dots$, and the output stream of the virtual encoder is $r[1]r[2]r[3]r[4]\dots$.

Compared with conventional convolutional encoders, the extended virtual encoder for MUD-XOR has three main different features: **1)** The MUD-XOR virtual encoder adopts arithmetic sum rather than the bit-wise ‘XOR’ operation. **2)** The MUD-XOR virtual encoder has several encoding coefficients H_1 , H_2 and H_3 . The values of these coefficients vary according to the property of the output samples $r[n]$, as follows:

$$\begin{aligned} H_1 &= \rho_{aa}^0, & H_2 &= \rho_{aa}^1 \text{ and } H_3 = \rho_{ab} & n &= 1, 3, 5, \dots \\ H_1 &= \rho_{bb}^0, & H_2 &= \rho_{bb}^1 \text{ and } H_3 = \rho_{ba} & n &= 2, 4, 6, \dots \end{aligned} \quad (19)$$

3) The code rate of the virtual encoder is 1. That is, there is no coding redundancy at all. Inspired by the virtual convolutional encoder, we adopt a Viterbi-like decoding algorithm to obtain each pair of original symbols $x_A[n]$ and $x_B[n](n = 1, 2, \dots, N)$. The decoding procedure is similar to the G-CRESM scheme proposed in [11]. Readers are referred to [11] for further details. In this paper, we extend the G-CRESM algorithm for the multipath scenario. After decoding individual symbols $x_A[n]$ and $x_B[n]$ from two end nodes, the relay R then constructs a downlink network-coded symbol $x_R[n] = x_A[n] \oplus x_B[n]$.

C. BER Performance Evaluation

Let L , Δ and ϕ denotes the number of paths in the channel between an end node and the relay, the symbol offset between two first paths and the relative phase rotations to the first path of node A, respectively. Fig. 5 plots the BER performance of the relay node using BPSK and QPSK modulations for both the double and quadruple sampling methods. The x-axis is the average per-bit SNR (its unit is dB) of the two paths and the y-axis is the average BER. In order to study the performance of the proposed MP-PNC algorithm, we choose synchronous PNC over a single-path AWGN channel and the extended disjoint MUD-XOR scheme with the same multipath channel (see (18)) as benchmarks. From the Fig. 5, we can see that compared with synchronous PNC (whose BER serves as lower inner-bound), the performance penalty of the MP-PNC decoding algorithm in a two-tap channel model

is only approximately 0.5dB. Moreover, it outperforms the MUD-XOR scheme by 3dB. In addition, quadruple sampling leads to better performance than double sampling. Note that we use a rectangular pulse shaping function, which is not band-limited. Therefore, quadruple sampling beyond the Nyquist rate will provide more information for computing *a posteriori* probability. Fig. 6 provides BER performance for the three-tap channel model. We use the double sampling method in this scenario. The gap between the synchronous case and the multipath case is less than 1 dB. We can also see that the BP-based algorithm has much better performance than the MUD-XOR scheme.

We consider the impact of different symbol misalignments on the BER performance in Fig. 7. We can find that the optimal value of Δ is 0.5, for both the BPSK and the QPSK modulation. With reference to Fig. 7 and Fig. 8 in [2], there are "good" and "bad" constellation points in the presence of phase offset. The bad points have greater possibilities to incur incorrect decisions. When the BP algorithm is carried out at the relay, the decision making for each XOR symbols is influenced by two adjacent symbols. Each of these two symbols (odd and even) is assigned a probability vector according to their time duration that depends on the degree of symbol misalignment (see (9) and (10)). Unequal durations result in a greater chance to place the degree of belief on a bad constellation point. Therefore, if Δ equals to 0.5, equally weighted probabilities lead into smaller number of wrong decisions than the other cases.

In asynchronous PNC, the constellation map of the joint symbols changes due to the random phase rotation. In [2], the authors analyzed the XOR mapping for the QPSK case at the relay node and pointed out that the worst case occurred when the phase rotation was $\pi/4$. If the phase rotation is around $\pi/4$, the XOR mapping method will perform poorly. Fig. 8 shows the influence of the different phase rotations on the BER curves. A larger phase rotation leads to worse performance. However, for the QPSK case, if we use another mapping method in the case where the phase rotation is in the range of $[\pi/4, 3\pi/4]$, the performance will be improved. The mapping rule is:

$$x_R^{Re}[n] = x_A^{Re}[n] \oplus x_B^{Im}[n], \quad x_R^{Im}[n] = x_A^{Im}[n] \oplus x_B^{Re}[n], \quad (20)$$

where the superscript *Re* and *Im* stand for the real and imaginary components of the symbols. Here, we do Re-IM XOR rather than Re-Re and IM-Re XORs. We shall refer to (20) as quadrature XOR mapping and the original scheme simply as XOR mapping.

We compare quadrature XOR mapping with XOR mapping in Fig. 8(b). From the figure,

we can see that quadrature XOR mapping improves BER by about 1 dB, very close to the synchronous case. We remark that this mapping rule is optimal only if the relative phase shift is in the range of $[\pi/4, 3\pi/4]$. If the value of phase shift is in other ranges, such as $[3\pi/4, 5\pi/4]$ or $[5\pi/4, 7\pi/4]$, we have to use another mapping (i.e., negative XOR mapping given by (21) or negative quadrature XOR mapping given by (22) as follows) to ensure the best system performance.

$$x_R^{Re}[n] = x_A^{Re}[n] \oplus (-x_B^{Re}[n]), \quad x_R^{Im}[n] = x_A^{Im}[n] \oplus (-x_B^{Im}[n]). \quad (21)$$

$$x_R^{Re}[n] = x_A^{Re}[n] \oplus (-x_B^{Im}[n]), \quad x_R^{Im}[n] = x_A^{Im}[n] \oplus (-x_B^{Re}[n]). \quad (22)$$

V. CONCLUSION AND FUTURE WORK

This paper has proposed an optimal maximum-likelihood (ML) decoder for physical-layer network coding (PNC) over multipath flat fading channel, referred to as MP-PNC, in a two-way relay network. The decoding algorithm is based on belief propagation (BP). Instead of regarding the signals from non-major paths as interferences, MP-PNC can fully exploit the fading coefficients from non-major channel paths for decoding the PNC packet. Therefore, it effectively improves the BER performance of the multipath system, compared with conventional disjoint MUD-XOR decoding algorithm. Specifically, simulation results show that with BP decoding, the phase asynchrony and multipath fading issue can be solved in an integrated manner. Moreover, if the phase rotation is larger than $\pi/4$, by changing the XOR mapping to a quadrature XOR mapping, we can improve the performance.

This work has only studied non-channel-coded PNC systems. Going forward, the study of channel-coded PNC under the multipath fading scenario will be interesting. In addition, investigation of PNC via a large delay multipath fading channel is also worthwhile.

REFERENCES

- [1] S. Zhang, S. C. Liew, and P. P. Lam, "Hot topic: Physical layer network coding," in *Proc. ACM MOBICOM*, 2006.
- [2] L. Lu, S. C. Liew, and S. Zhang, "Optimal decoding algorithm for asynchronous physical-layer network coding," in *Proc. IEEE Int. Conf. on Comm. (ICC)*, June 2011.
- [3] L. Lu and S. C. Liew, "Asynchronous physical-layer network coding," *IEEE Trans. Wireless Commun.*, vol. 11, no. 2, Feb. 2012.
- [4] S. Zhang, S. C. Liew, and H. Wang, "Synchronization analysis in physical layer network coding," available at: <http://arxiv.org/ftp/arxiv/papers/1001/1001.0069.pdf>.
- [5] U. Bhat and T. M. Duman, "Decoding strategies for physical-layer network coding over frequency selective channels," in *Proc. IEEE Wireless Comm. and Net. Conf.*, Apr. 2012.

- [6] F. Rossetto and M. Zorzi, "A practical architecture for ofdm-based decode-and-forward physical-layer network coding," *IEEE Trans. Signal Processing*, vol. 60, no. 9, Sept. 2012.
- [7] L. Lu, , T. T. Wang, S. C. Liew, and S. Zhang, "Implementation of physical-layer network coding," *Physical Communication*, vol. 6, no. 1, pp. 74–87, Mar. 2013.
- [8] X. Xia, K. Xu, and Y. Xu, "Asynchronous physical-layer network coding scheme for two-way ofdm relay," available at: <http://arxiv.org/abs/1204.2692>, Apr. 2012.
- [9] *ITU-R Recommendation M.1225*, Std., 1997.
- [10] F. R. Kschischang, B. J. Frey, and H.-A. Loeliger, "Factor graphs and the sum-product algorithm," *IEEE Trans. Information Theory*, vol. 47, no. 2, Feb. 2001.
- [11] L. Lu, S. C. Liew, and S. Zhang, "Collision resolution by exploiting symbol misalignment," available at: <http://arxiv.org/abs/0810.0326>.

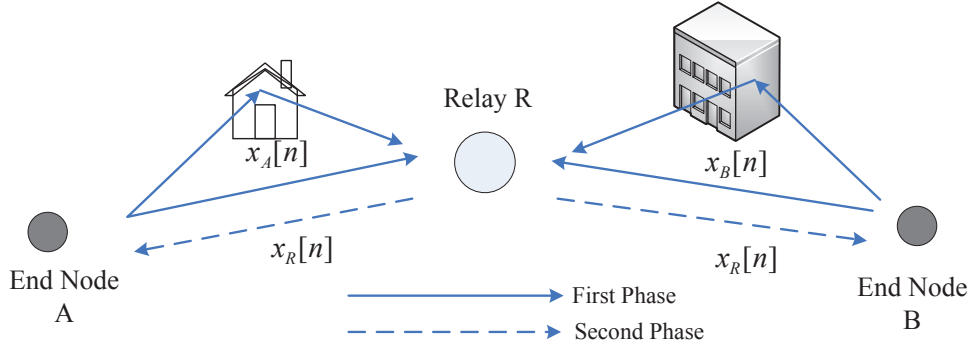


Fig. 1: System model for two way relay channel.

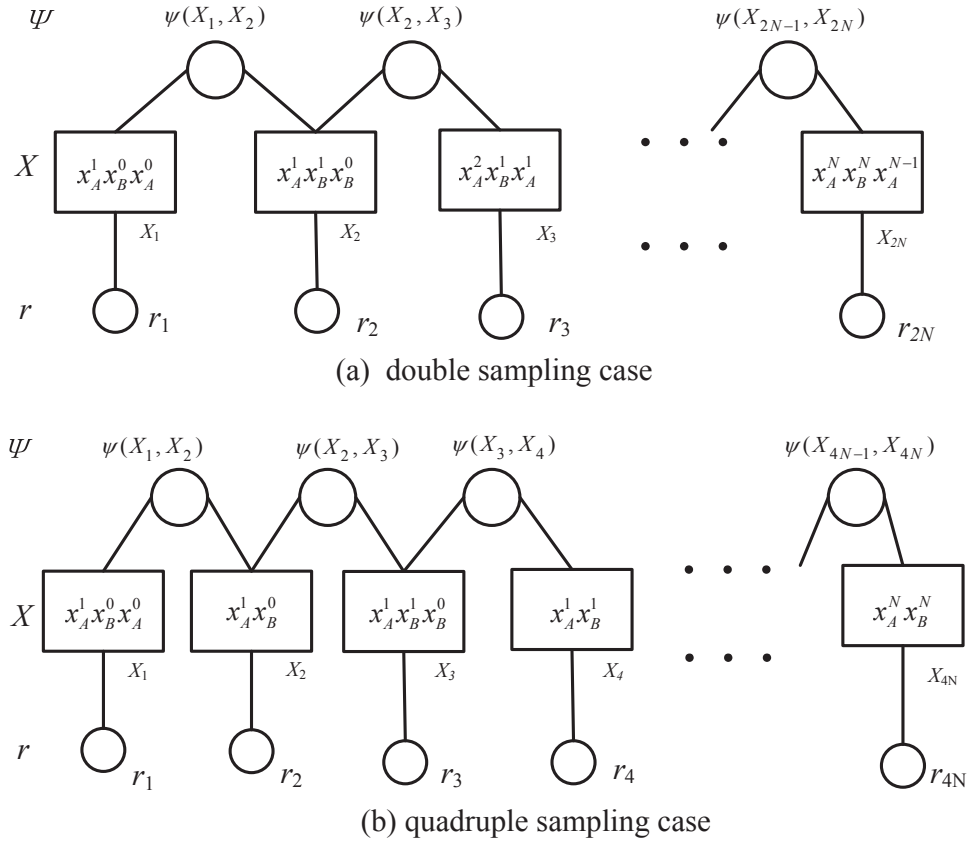


Fig. 2: Tanner graph constructed for MP-PNC joint decoding.

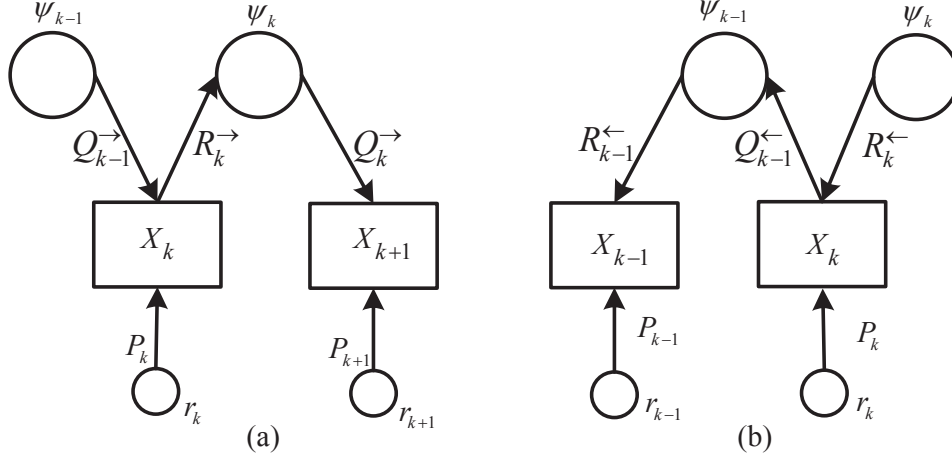


Fig. 3: (a)From left to right; (b)From right to left.
Message updating rules in Tanner graph.

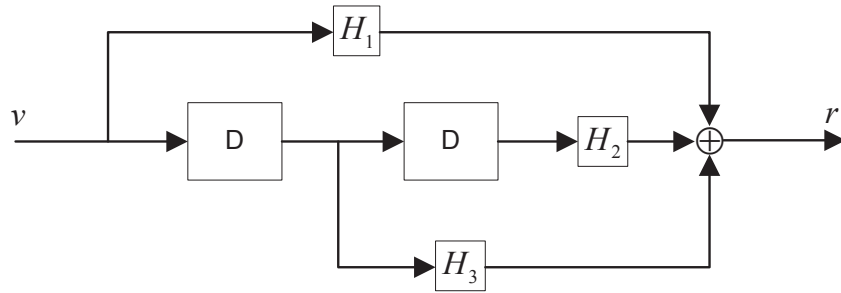


Fig. 4: The virtual encoder for MUD-XOR system, where D stands for one symbol delay.

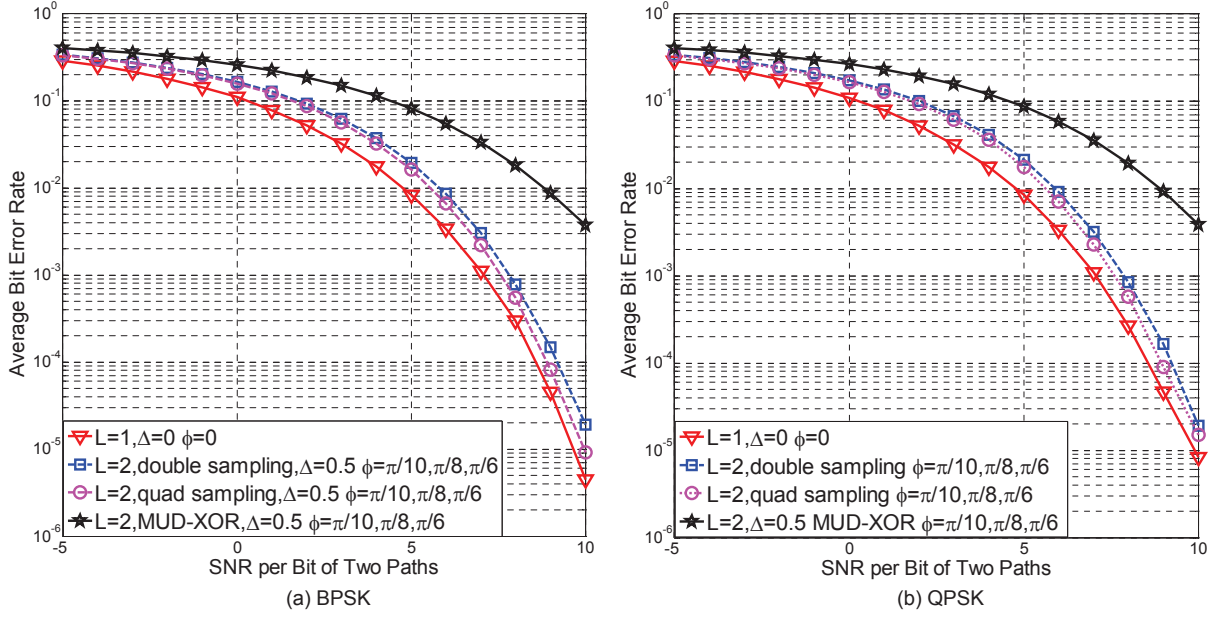


Fig. 5: BER curves for MP-PNC decoding in a two-tap multipath channel: (a) BPSK; (b) QPSK. L denotes the number of paths, Δ denotes the symbol offset between the two first paths from the two end nodes, and ϕ represents the relative phase rotation of other paths with respect to the first path of end node A .

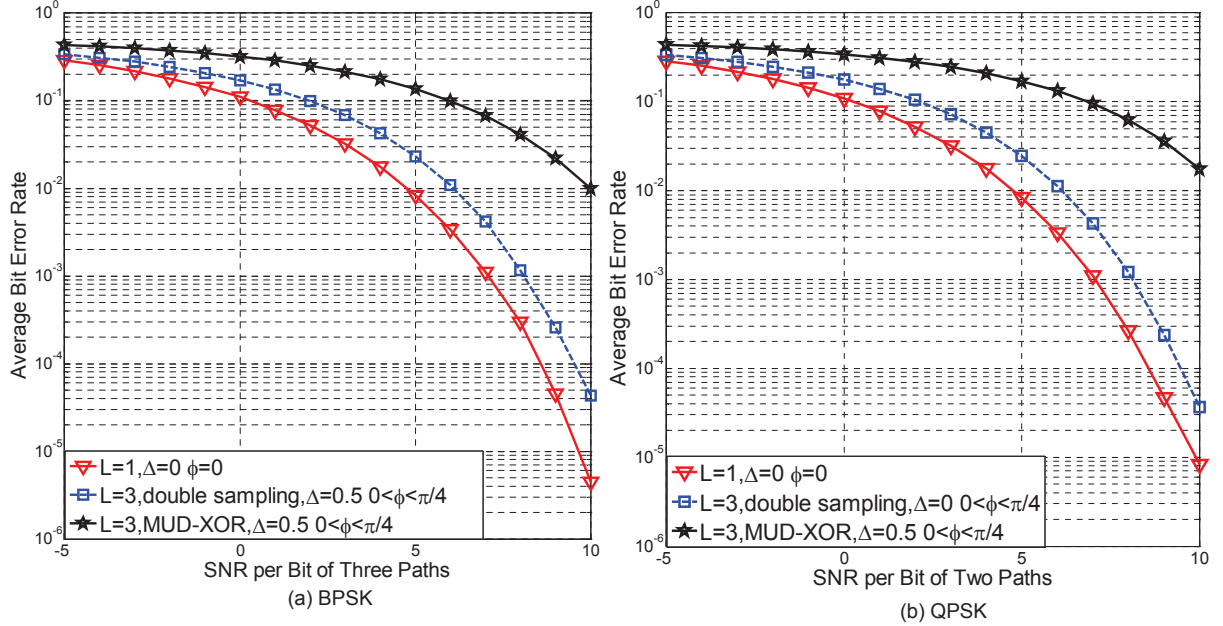


Fig. 6: PNC via a three-tap multipath channel.

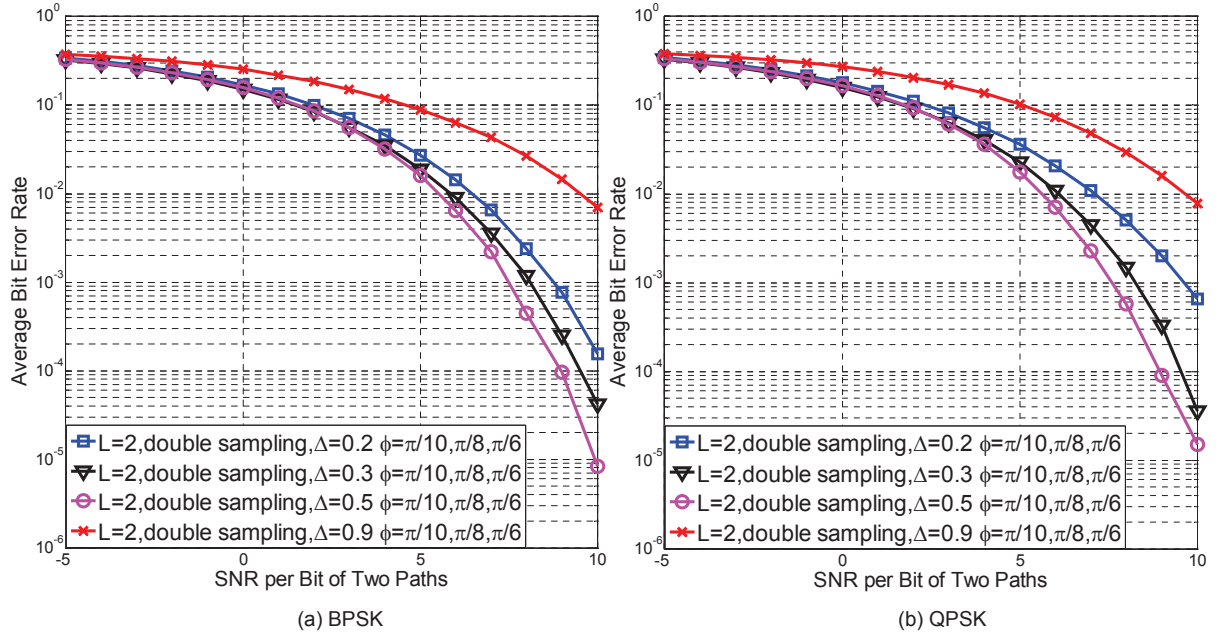


Fig. 7: BER performance with different symbol misalignments.

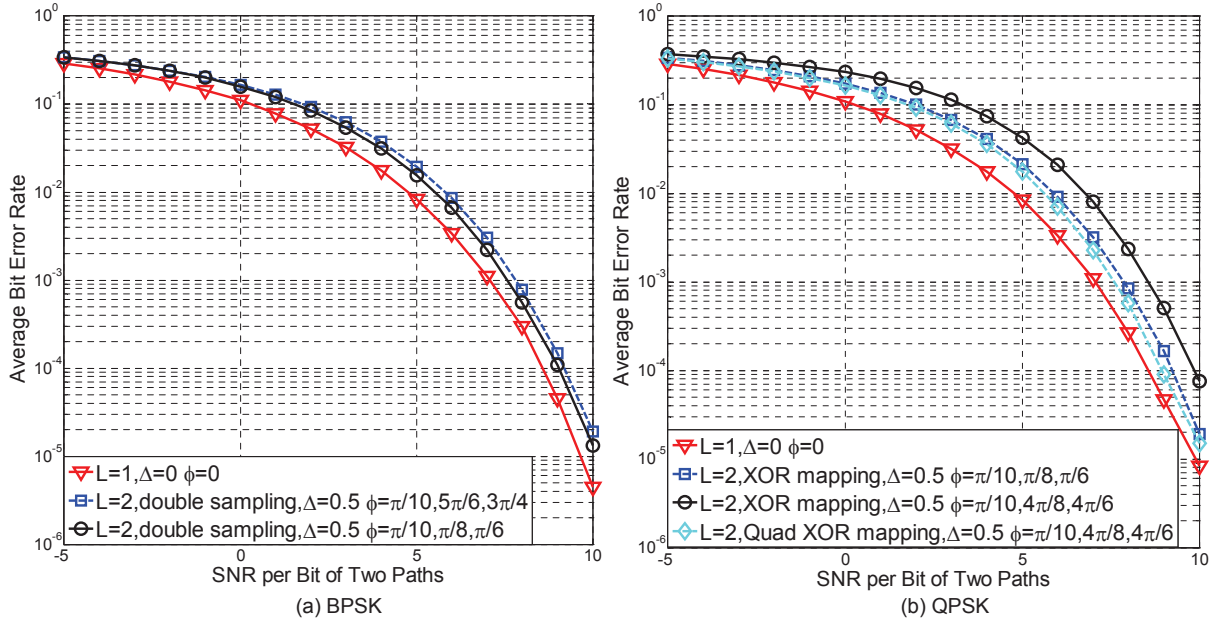


Fig. 8: BER performance with different phase rotations and mappings: for the Quad XOR mapping curve in QPSK case, we choose quadrature XOR mapping rule described by (20), since the relative phase rotations are within the range of $[\pi/4, 3\pi/4]$.